

# Analytical and numerical study of hardcore bosons in two dimensions

K. Bernardet, G. G. Batrouni, J.-L. Meunier

*Institut Non-Linéaire de Nice, Université de Nice-Sophia Antipolis, 1361 route des Lucioles, 06560 Valbonne, France*

G. Schmid, M. Troyer

*Theoretische Physik, Eidgenössische Technische Hochschule Zürich, CH-8093 Zürich, Switzerland*

A. Dorneich

*Institut für Theoretische Physik, Universität Würzburg, 97074 Würzburg, Germany*

We study various properties of bosons in two dimensions interacting only via onsite hardcore repulsion. In particular, we use the lattice spin-wave approximation to calculate the ground state energy, the density, the condensate density and the superfluid density in terms of the chemical potential. We also calculate the excitation spectrum,  $\omega(\mathbf{k})$ . In addition, we performed high precision numerical simulations using the stochastic series expansion algorithm. We find that the spin-wave results describe extremely well the numerical results over the *whole* density range  $0 \leq \rho \leq 1$ . We also compare the lattice spin-wave results with continuum results obtained by summing the ladder diagrams at low density. We find that for  $\rho \leq 0.1$  there is good agreement, and that the difference between the two methods vanishes as  $\rho^2$  for  $\rho \rightarrow 0$ . This offers the possibility of obtaining precise continuum results by taking the continuum limit of the spin-wave results for all densities. Finally, we studied numerically the finite temperature phase transition for the entire density range and compared with low density predictions.

PACS numbers: 05.30.Jp, 67.40.Yv, 74.60.Ge, 75.10.Nr

(November 4, 2018)

## I. INTRODUCTION

The calculation of the thermodynamic properties of dilute Bose gases is an old problem that keeps attracting renewed attention. Of particular interest is the ground state energy per particle,  $\epsilon(\rho)$ , where  $\rho$  is the density of particles. The three dimensional case, with hardcore repulsive interaction, was first treated by Bogoliubov<sup>1</sup>. This was later elaborated by many other authors<sup>2</sup> using a variety of methods. The main result is that the leading term in the ground state energy per particle (in three dimensions) is  $\epsilon(\rho) = 4\pi\rho a(\hbar^2/2m)$ , where  $m$  is the mass of the particle and  $a$  the scattering length. For hardcore bosons,  $a$  is simply the diameter of the particles. This result was recently demonstrated rigorously by Lieb and Yngvason.<sup>3</sup> The first two corrections to this result have also been calculated.

Clearly, this result cannot be true in two dimensions since the units would be incorrect. The units would work out if one eliminates the dependence on the scattering length  $a$ , i.e. the hardcore boson diameter. However, it is not reasonable to expect the energy to be independent of the scattering length. The solution to this problem was provided by Schick<sup>4</sup> in 1971 who used the field theoretic methods developed and applied by Beliaev<sup>2</sup> to the three dimensional problem. This method, which applies in the very dilute limit, consists of assuming that the dominant contributions come from ladder diagrams which are then summed. Schick found that the leading contribution to the energy per parti-

cle is  $\epsilon(\rho) = 4\pi\rho(\hbar^2/2m)|\ln(\rho a^2)|^{-1}$  with the first correction being proportional to  $(\ln(\rho a^2))^{-1}$ . Hines *et al* re-analyzed<sup>5</sup> the integral obtained by Schick and found that the first correction term is larger and is equal to  $-\ln|\ln(\bar{\rho})|/|\ln(\bar{\rho})|$  where  $\bar{\rho} = \rho a^2/\pi$ . Lieb and Yngvason<sup>3</sup> proved rigorously that the leading contribution to the energy is indeed the term calculated by Schick, and that the leading correction<sup>6</sup> is between  $\mathcal{O}(|\ln(\rho a^2)|^{-1})$  and  $\mathcal{O}(|\ln(\rho a^2)|^{-1/5})$  which is consistent with the correction calculated by Hines *et al*.

As mentioned above, these results are for very small densities.

In the meantime interest in hardcore bosons on two dimensional lattices has been on the rise<sup>7-11</sup> and simulation algorithms have been improving dramatically.

In this paper we will study in detail hardcore bosons on a two dimensional square lattice. Our approach is to do very high precision numerical simulations using the stochastic series expansion (SSE) algorithm<sup>12,13</sup> and mean field plus spin-wave analyses. The quantities we calculate and measure with simulations are: The density,  $\rho$ , as a function of the chemical potential,  $\mu$ , the condensate,  $\rho_0(\mu)$ , the energy,  $\epsilon(\mu)$ , the excitation spectrum and  $\omega(\vec{k})$ . In addition, by twisting the boundary conditions, the spin-wave calculation also yields the superfluid density as a function of  $\mu$  (or  $\rho$ ). The numerical simulations are done at very low temperature (essentially  $T = 0$ ) mostly on  $32 \times 32$  systems with some  $48 \times 48$  results. We study these systems from very low densities up to half filling, which is equivalent to studying the entire

density range  $[0, 1]$  due to the particle-hole symmetry.

Our goal is to determine the range of densities for which the spin-wave and continuum calculations are reliable. In addition we are interested in whether and how the spin-wave calculation converges to the continuum calculation (summation of ladder diagrams).

The paper is organized as follows. In section **II** we present, in some detail, the mean field and spin-wave calculations of the various physical quantities at  $T = 0$ . In section **III** we compare the zero temperature numerical results with the results of section **II**. In section **IV** we compare the spin-wave calculation with the continuum ladder diagram results valid for low densities. In section **V** we briefly examine finite temperatures and finally, in section **VI** we present some conclusions and comments.

## II. MEAN FIELD AND SPIN-WAVES

We will consider a two dimensional system of hardcore bosons on an  $L \times L$  lattice. The hamiltonian is given by

$$H = -t \sum_{\langle ij \rangle} (a_i^\dagger a_j + a_j^\dagger a_i) - \mu \sum_i \hat{n}_i. \quad (1)$$

where  $\langle ij \rangle$  denotes near neighbors,  $a_i$  ( $a_i^\dagger$ ) destroys (creates) a boson on site  $i$ , and  $\mu$  is the chemical potential. The hopping parameter,  $t$ , sets the energy scale and will be set equal to one in the simulations. In addition, of course, the hardcore constraint should be enforced. This means that the number of bosons on a given site,  $i$ , as measured by the number operator,  $\hat{n}_i = a_i^\dagger a_i$ , can only be 0 or 1. This is not convenient to express in terms of the bosonic operators since the normal commutation relations allow any number of bosons on a given site.

To enforce the hardcore constraint in a simple way, we exploit the exact mapping between this system and the two dimensional antiferromagnetic Heisenberg model:  $a_i^\dagger \leftrightarrow S_i^+$ ,  $a_i \leftrightarrow S_i^-$ , and  $\hat{n}_i \leftrightarrow S_i^z + 1/2$ . With this mapping the hardcore boson Hubbard hamiltonian becomes

$$H = -t \sum_{\langle ij \rangle} (S_i^+ S_j^- + S_i^- S_j^+) - \mu \sum_i S_i^z - \frac{\mu}{2} N, \quad (2)$$

where  $N = L \times L$  is the total number of sites.

We start with the mean field calculation.

### A. Mean field

The mean field calculation proceeds in the conventional way<sup>14</sup>. The lowest possible energy state corresponds to all spins down (no bosons):  $|0\rangle = \prod_i |\downarrow\rangle_i$  and a total magnetization of  $-N/2$ . Increasing  $\mu$  to add bosons corresponds to increasing the externally applied magnetic field in the positive  $z$  direction. In the mean field solution, we take all spins parallel and making an angle

$\theta$  with the positive  $z$  axis. When the system is empty  $\theta = \pi$ , and the (site independent) azimuthal angle  $\phi$  is 0 for the moment. Increasing the chemical potential (magnetic field) the spins will turn to reduce the angle with the  $z$  axis. The mean field state vector is then

$$|\psi\rangle = \prod_i (u + v S_i^+) |0\rangle, \quad (3)$$

where  $u = \sin(\theta/2)$  is the amplitude for the spin to be down, and  $v = \cos(\theta/2)$  the amplitude for an up spin. The total  $z$  spin is  $S_z = S \cos(\theta) = N_b - N/2$  where  $S$  is the largest possible total spin ( $= N/2$ ) and  $N_b$  is the total number of bosons. These equations yield the relation between the particle density,  $\rho = N_b/N$ , and the angle  $\theta$ :

$$\sin^2(\theta) = 4\rho(1 - \rho). \quad (4)$$

Several quantities can now be readily calculated as functions of  $\rho$  or  $\theta$ . The expectation value of the hamiltonian in the mean field state,  $|\psi\rangle$ , can be easily calculated and gives the free energy per site,  $F$  (recall that we are using the grand canonical ensemble),

$$F = -t \sin^2(\theta) - \frac{\mu}{2} \cos(\theta) - \frac{\mu}{2}. \quad (5)$$

To determine the dependence of the chemical potential on the angle  $\theta$  we minimize  $F$ ,  $\partial F / \partial \theta = 0$ . This yields

$$\cos(\theta) = \frac{\mu}{4t}, \quad (6)$$

which, when used with Eq. 4, gives the particle density in terms of the chemical potential,

$$\rho = \frac{1}{2} + \frac{\mu}{8t}. \quad (7)$$

Therefore,  $F$  becomes,

$$\begin{aligned} F &= -4t\rho^2, \\ &= -t \left(1 + \frac{\mu}{4t}\right)^2. \end{aligned} \quad (8)$$

In the ground state, the internal energy (per site),  $E$ , which is what is measured numerically, is related to the free energy via the expression

$$\begin{aligned} E &= F + \mu \langle \rho \rangle, \\ &= -t + t \left(\frac{\mu}{4t}\right)^2, \\ &= -4\rho t(1 - \rho), \end{aligned} \quad (9)$$

where we used Eqs. 6 and 7.

The density of particles in the zero momentum mode (the condensate) is given by:

$$\begin{aligned} \rho_0 &= \frac{1}{N} \langle \psi | \tilde{a}^\dagger(\mathbf{k}=0) \tilde{a}(\mathbf{k}=0) | \psi \rangle, \\ &= \frac{1}{N} \sum_{i,j} \langle \psi | S_i^+ S_j^- | \psi \rangle, \\ &= \rho(1 - \rho), \\ &= \frac{1}{4} \left(1 - \left(\frac{\mu}{4t}\right)^2\right), \end{aligned} \quad (10)$$

where the operators  $\tilde{a}^\dagger(\mathbf{k})$  ( $\tilde{a}(\mathbf{k})$ ) are Fourier transforms of  $a_i^\dagger$  ( $a_i$ ).

These results will be compared with the simulation results below. First we calculate the spin-wave corrections.

## B. Spin-waves

To include spin-wave corrections, we proceed the usual way<sup>7,15,8,9</sup>. We first rotate the  $z$ -axis to align it with the mean field magnetization direction, *i.e.* ( $\phi = 0, \theta$ ). This is accomplished by the rotations

$$\begin{aligned} S_i^x &= S_i'^x \cos(\theta) + S_i'^z \sin(\theta), \\ S_i^y &= S_i'^y, \\ S_i^z &= -S_i'^x \sin(\theta) + S_i'^z \cos(\theta), \end{aligned} \quad (11)$$

where  $\vec{S}_i'$  is the spin vector in the rotated frame. Equation 2 becomes

$$\begin{aligned} H = -2t \sum_{\langle ij \rangle} & \left( (S_i'^x S_j'^x \cos^2(\theta) + 2S_i'^x S_j'^z \cos(\theta) \sin(\theta) \right. \\ & \left. + S_i'^z S_j'^z \sin^2(\theta)) + S_i'^y S_j'^y \right) - \mu \sum_i \left( -S_i'^x \sin(\theta) \right. \\ & \left. + S_i'^z \cos(\theta) \right) - \frac{\mu}{2} N. \end{aligned} \quad (12)$$

Now, the spins in the rotated frame are expressed in terms of bosonic operators  $b_i^\dagger$  and  $b_i$ . These operators do *not* describe the original hardcore bosons, Eq. 1. Instead they describe the low energy bosonic fluctuations, the spin-waves. As such, they obey the usual bosonic commutation relations,  $[b_i, b_j^\dagger] = \delta_{i,j}$ . This transformation is accomplished by using

$$\begin{aligned} S_i'^x &= \frac{1}{2}(S_i'^+ + S_i'^-) = \frac{1}{2}(b_i^\dagger + b_i), \\ S_i'^y &= \frac{1}{2i}(S_i'^+ - S_i'^-) = \frac{1}{2i}(b_i^\dagger - b_i), \\ S_i'^z &= \frac{1}{2} - b_i^\dagger b_i. \end{aligned} \quad (13)$$

Substituting these expressions in Eq. 12, we assume a dilute gas of spin-waves and ignore cubic and quartic terms in the bosonic operators. This yields,

$$\begin{aligned} H = -\frac{t}{2} \sum_{\langle ij \rangle} & \left( -\sin^2(\theta)(b_i^\dagger b_j^\dagger + b_i b_j) \right. \\ & \left. + (1 + \cos^2(\theta))(b_i^\dagger b_j + b_i b_j^\dagger) \right) \\ & + (4t \sin^2(\theta) + \mu \cos(\theta)) \sum_i b_i^\dagger b_i \\ & - N \left( \frac{\mu}{2}(1 + \cos(\theta)) + t \sin^2(\theta) \right) \\ & + (-2t \cos(\theta) + \frac{\mu}{2}) \sin(\theta) \sum_i (b_i^\dagger + b_i). \end{aligned} \quad (14)$$

The term linear in the operators is required to vanish yielding,

$$\cos(\theta) = \frac{\mu}{4t}. \quad (15)$$

This is the same relation between  $\theta$  and  $\mu$  we found in the mean field case: Spin-waves do not modify it.

We are, therefore, left with a quadratic hamiltonian which we can diagonalize by first going to Fourier space,

$$\begin{aligned} b_{\mathbf{r}}^\dagger &= \frac{1}{\sqrt{N}} \sum_{\mathbf{k}} e^{-i\mathbf{k} \cdot \mathbf{r}} b_{\mathbf{k}}^\dagger, \\ b_{\mathbf{r}} &= \frac{1}{\sqrt{N}} \sum_{\mathbf{k}} e^{i\mathbf{k} \cdot \mathbf{r}} b_{\mathbf{k}}. \end{aligned} \quad (16)$$

This give,

$$\begin{aligned} H = H_{MF} + \sum_{\mathbf{k}} & \left( A_{\mathbf{k}} (b_{\mathbf{k}}^\dagger b_{\mathbf{k}} + b_{-\mathbf{k}}^\dagger b_{-\mathbf{k}}) \right. \\ & \left. + B_{\mathbf{k}} (b_{\mathbf{k}}^\dagger b_{-\mathbf{k}}^\dagger + b_{\mathbf{k}} b_{-\mathbf{k}}) \right), \end{aligned} \quad (17)$$

where,

$$\begin{aligned} A_{\mathbf{k}} &= -\frac{t}{2} \left( (1 + (\frac{\mu}{4t})^2) \gamma_{\mathbf{k}} - 4 \right), \\ B_{\mathbf{k}} &= \frac{t}{2} \left( 1 - (\frac{\mu}{4t})^2 \right) \gamma_{\mathbf{k}}, \\ \gamma_{\mathbf{k}} &= \cos(k_x) + \cos(k_y). \end{aligned} \quad (18)$$

$H_{MF}$  is the constant term in Eq. 14, which is identical to Eq. 5. Eliminating  $\theta$  by using Eq. 15 we get the second of Eq. 8. In other words,  $H_{MF}$  is just the pure mean field result.

To diagonalize the quadratic spin-wave hamiltonian, Eq. 17, we use the Bogoliubov transformation,

$$b_{\mathbf{k}} = u_{\mathbf{k}} \alpha_{\mathbf{k}} - v_{\mathbf{k}} \alpha_{-\mathbf{k}}^\dagger, \quad b_{\mathbf{k}}^\dagger = u_{\mathbf{k}} \alpha_{\mathbf{k}}^\dagger - v_{\mathbf{k}} \alpha_{-\mathbf{k}}, \quad (19)$$

where  $\alpha_{\mathbf{k}}^\dagger$  ( $\alpha_{\mathbf{k}}$ ) is a creation (destruction) operator for a quasi-particle excitation of momentum  $\mathbf{k}$ . These operators satisfy the bosonic commutation relation,  $[\alpha_{\mathbf{k}}, \alpha_{\mathbf{k}'}^\dagger] = \delta_{\mathbf{k}, \mathbf{k}'}$ , if  $u_{\mathbf{k}}^2 - v_{\mathbf{k}}^2 = 1$ . We can ensure this by writing,

$$u_{\mathbf{k}} = \cosh(\phi_{\mathbf{k}}), \quad v_{\mathbf{k}} = \sinh(\phi_{\mathbf{k}}), \quad (20)$$

where  $\phi_{\mathbf{k}}$  is determined by the requirement the Bogoliubov transformation diagonalize the hamiltonian, Eq. 17.

We, therefore, obtain

$$\begin{aligned} \sinh^2(\phi_{\mathbf{k}}) &= \frac{1}{2} \left( \frac{A_{\mathbf{k}}}{\sqrt{A_{\mathbf{k}}^2 - B_{\mathbf{k}}^2}} - \frac{1}{2} \right), \\ \cosh^2(\phi_{\mathbf{k}}) &= \frac{1}{2} \left( \frac{A_{\mathbf{k}}}{\sqrt{A_{\mathbf{k}}^2 - B_{\mathbf{k}}^2}} + \frac{1}{2} \right), \end{aligned} \quad (21)$$

with  $A_{\mathbf{k}}$  and  $B_{\mathbf{k}}$  given by Eq. 18. The diagonalized spin-wave hamiltonian then becomes,

$$H = \left( H_{MF} + \sum_{\mathbf{k}} (\sqrt{A_k^2 - B_k^2} - A_k) \right) + \sum_{\mathbf{k} \neq 0} \sqrt{A_k^2 - B_k^2} (\alpha_{\mathbf{k}}^\dagger \alpha_{\mathbf{k}} + \alpha_{-\mathbf{k}}^\dagger \alpha_{-\mathbf{k}}). \quad (22)$$

This immediately gives the spin-wave corrected free energy per site,  $F_{SW}$ ,

$$F_{SW} = -t \left( 1 + \left( \frac{\mu}{4t} \right)^2 \right) + \frac{1}{N} \sum_{\mathbf{k}} (\sqrt{A_k^2 - B_k^2} - A_k), \quad (23)$$

where we wrote explicitly the expression for  $H_{MF}$  using Eq. 8. Equation 22 also gives the dispersion of quasi-particle excitations,

$$\omega(\mathbf{k}) = 2\sqrt{A_k^2 - B_k^2}. \quad (24)$$

It is easy to show, using Eqs. (18,24), that as  $\mathbf{k} \rightarrow 0$ , we obtain the linear dispersion characteristic of phonons,

$$\omega(\mathbf{k} \rightarrow 0) = 2t\sqrt{1 - \left( \frac{\mu}{4t} \right)^2} |\mathbf{k}|. \quad (25)$$

This gives the sound speed (critical velocity) as

$$c = 2t\sqrt{1 - \left( \frac{\mu}{4t} \right)^2}. \quad (26)$$

Now that we have diagonalized the hamiltonian, we can calculate the spin-wave corrections to the quantities already obtained by mean field. The number of particles kicked out of the condensate ( $\mathbf{k} = 0$  mode) due to the spin-waves is given by  $n_{\mathbf{k}} = \langle \psi | b_{\mathbf{k}}^\dagger b_{\mathbf{k}} | \psi \rangle$ . Using Eq. 19 and the fact that  $\alpha_{\mathbf{k}} | \psi \rangle = 0$  (no quasi-particle excitations in the ground state), we get,

$$n_{\mathbf{k} \neq 0} = \frac{1}{2} \left( \frac{A_k}{\sqrt{A_k^2 - B_k^2}} - \frac{1}{2} \right). \quad (27)$$

The spin-wave corrected condensate density is then,

$$\rho_0 = \rho(1 - \rho) - \frac{1}{N} \sum_{\mathbf{k} \neq 0} n_{\mathbf{k}}. \quad (28)$$

Whereas spin-waves did not modify the relation between  $\mu$  and  $\theta$ , they do introduce a correction to the relation between  $\mu$  and  $\rho$ . To find the new expression, we simply use  $\rho = -\partial F_{SW} / \partial \mu$ . This gives

$$\rho = \frac{1}{2} \left( 1 + \frac{\mu}{4t} \right) + \frac{1}{N} \frac{\mu}{16t} \sum_{\mathbf{k} \neq 0} \gamma_{\mathbf{k}} \left( \frac{A_k - B_k}{\sqrt{A_k^2 - B_k^2}} - 1 \right). \quad (29)$$

Now that we have determined  $F_{SW}$  and  $\rho(\mu)$ , we can calculate the boson energy per site (internal energy),  $E$ , using  $E_{SW} = F_{SW} + \mu \langle \rho \rangle$ . This gives,

$$E_{SW} = -t \left( 1 - \left( \frac{\mu}{4t} \right)^2 \right) + \frac{1}{N} \sum_{\mathbf{k} \neq 0} (\sqrt{A_k^2 - B_k^2} - A_k) + \frac{t}{N} \left( \frac{\mu}{4t} \right)^2 \sum_{\mathbf{k} \neq 0} \gamma_{\mathbf{k}} \left( \frac{A_k - B_k}{\sqrt{A_k^2 - B_k^2}} - 1 \right). \quad (30)$$

### C. Superfluid density

Unlike the above thermodynamic quantities, the superfluid density,  $\rho_s$ , requires special treatment of the boundary conditions. As is well known<sup>16</sup>, one can relate  $\rho_s$  to the “spin stiffness”. To accomplish this, we need to compare the free energy of the system under periodic and twisted boundary conditions. This energy difference is related to  $\rho_s$ .

In the periodic case, which we treated above, the azimuthal angle,  $\phi$ , was taken to be site independent (equal to zero). To implement a twist, we take this angle to be site dependent,  $\phi_{\mathbf{r}}$ , and with a constant gradient such that the total twist across the system in both the  $x$  and  $y$  directions is  $2\pi$ ,

$$\delta\phi = \phi_{\mathbf{r}+\hat{\mathbf{x}}} - \phi_{\mathbf{r}} = \phi_{\mathbf{r}+\hat{\mathbf{y}}} - \phi_{\mathbf{r}} = \frac{2\pi}{L}, \quad (31)$$

where  $\hat{\mathbf{x}}$  ( $\hat{\mathbf{y}}$ ) is a unit vector in the  $x$  ( $y$ ) direction. Consequently, the rotation of the reference frame to align it with the local spin will be site dependent,

$$\begin{aligned} S_i^x &= \left( S_i'^x \cos(\theta) + S_i'^z \sin(\theta) \right) \cos(\phi_i) - S_i'^y \sin(\phi_i), \\ S_i^y &= \left( S_i'^x \cos(\theta) + S_i'^z \sin(\theta) \right) \sin(\phi_i) + S_i'^y \cos(\phi_i), \\ S_i^z &= -S_i'^x \sin(\theta) + S_i'^z \cos(\theta). \end{aligned} \quad (32)$$

The rotation and diagonalization now proceed exactly as before giving,

$$\mu = 4t \cos(\theta) \cos(\delta\phi), \quad (33)$$

and

$$F_{SW}^T = -t \left( 1 + \left( \frac{\mu}{4t \cos(\delta\phi)} \right)^2 \right) + \frac{1}{N} \sum_{\mathbf{k}} (\sqrt{(A_k^T)^2 - (B_k^T)^2} - A_k^T), \quad (34)$$

where the  $T$  superscript indicates that the boundary conditions are twisted.  $A_k^T$  and  $B_k^T$  are given by

$$\begin{aligned} A_k^T &= -\frac{t}{2} \left( \left( 1 + \left( \frac{\mu}{4t \cos(\delta\phi)} \right)^2 \right) \gamma_{\mathbf{k}} - 4 \right), \\ B_k^T &= \frac{t}{2} \left( 1 - \left( \frac{\mu}{4t \cos(\delta\phi)} \right)^2 \right) \gamma_{\mathbf{k}}, \end{aligned} \quad (35)$$

and  $\gamma_{\mathbf{k}}$  has not changed.

We can now calculate  $\Delta F_{SW} = F_{SW}^T - F_{SW}$ ,

$$\Delta F_{SW} = \left( \rho(1 - \rho) + \frac{1}{tN} \sum_{\mathbf{k} \neq 0} \left( A_k - \sqrt{A_k^2 - B_k^2} \right) t \frac{(\delta\phi)^2}{2} \right), \quad (36)$$

where we made the approximation  $\cos(\delta\phi) \approx 1 - (\delta\phi)^2/2$ . The square of the gradient twist can be related to the kinetic energy of the superfluid<sup>16</sup> by

$$(\delta\phi)^2 = \frac{m^2}{2\hbar^2} v^2, \quad (37)$$

with  $v^2 = v_x^2 + v_y^2$ . Recalling that  $t = \hbar^2/(2m)$ , we obtain the superfluid density,

$$\rho_s = \rho(1 - \rho) + \frac{1}{tN} \sum_{\mathbf{k} \neq 0} \left( A_k - \sqrt{A_k^2 - B_k^2} \right). \quad (38)$$

It is very interesting to note that at the mean field level, the superfluid density and the condensate are identical,  $\rho_0 = \rho_s$  (see Eqs.(28,38)). As expected, spin-wave corrections deplete the condensate, Eq. 28, but surprisingly, the superfluid density is *enhanced* since the second term in Eq. 38 is positive. Furthermore, both our spin-wave calculation and numerical simulations (see below) show that even at zero temperature (the present case), the superfluid density is never truly equal to the density more to the condensate density. In fact, we always have  $\rho_s < \rho$  and, of course,  $\rho_s > \rho_0$ . It is worth noting that at the very small densities present in atomic condensates (of the order of  $10^{-4}$ ), our results do indeed yield  $\rho_s \approx \rho_0 \approx \rho$ , which agrees with the experimental observations.<sup>19</sup>

We now compare these results with numerical simulations.

### III. NUMERICAL SIMULATIONS

The numerical simulations were done using the SSE algorithm.<sup>12,13</sup> The results we will present here are for a  $32 \times 32$  system with periodic boundary conditions and inverse temperature  $\beta = 45$ . Since we are, mostly, interested in the zero temperature properties, we checked the finite temperature effects by doing simulations at  $\beta = 60$ . In addition, we checked the finite size effects by simulating  $48 \times 48$  systems. Within our very small error bars, the results were identical to the simulations for  $32 \times 32$  at  $\beta = 45$ . We can, therefore, consider these results to be valid in the thermodynamic limit at  $T = 0$ .

One of the quantities of prime interest is the superfluid density,  $\rho_s$ . In the previous section, we calculated  $\rho_s$  using the relation between the helicity modulus and the difference in free energies with periodic and antiperiodic

boundary conditions.<sup>16</sup> Numerically,  $\rho_s$  is determined from the winding number,<sup>17</sup>

$$\rho_s = \frac{m}{\hbar^2} \frac{\langle W^2 \rangle}{D\beta}, \quad (39)$$

where  $W$  is the winding number,  $D$  the dimensionality, and  $\beta = 1/k_B T$ . Since the hopping parameter  $t$  is related to the mass via  $t = \hbar^2/(2ma^2)$ , where  $a$  is the diameter of the hardcore boson (one lattice spacing in our case), Eq. 39 becomes

$$\rho_s = \frac{1}{2ta^2} \frac{\langle W^2 \rangle}{D\beta}. \quad (40)$$

In section V we will consider the finite temperature KT transition from superfluid to normal phases. This temperature from the superfluid density using the universal jump condition<sup>18</sup>,

$$\frac{\pi}{2} \rho_s = \frac{mk_B T_{KT}}{\hbar^2}, \quad (41)$$

with  $m$  related to  $t$  as above.

The spin-wave results contain momentum summations which we did numerically, typically for  $L = 32$ , to compare directly with the numerical simulations.

In Fig. 1 we show the bosonic energy,  $E$  as a function of the particle density,  $\rho$ . The circles are the numerical results, with error bars smaller than the size of the points. The dashed line shows the mean field result, Eq. 9, and the solid line shows the mean field plus spin-wave correction, Eq. 30. The long dashed line will be discussed in the next section. We see that agreement between the numerical and spin-wave results is excellent for the whole range of densities,  $0 \leq \rho \leq 0.5$ , and particle hole symmetry extends this agreement all the way to full filling.

Figure 2 shows the comparison of the condensate fraction,  $\rho_0$ , Eqs. 10 and 28 with the numerical results. The line convention is as for the previous figure. Once again we see that the agreement between spin-waves and simulations is remarkable over the entire density range. Numerically, the condensate fraction  $\rho_0$  was calculated as the Fourier transformed of the zero momentum equal time Greens function.

In Fig. 3 we show the dependence of the particle density on the chemical potential, Eqs. 7 and 29. Again we see that the agreement between the spin-wave calculation and the numerical simulation is excellent.

The superfluid density,  $\rho_s$  (Eq. 38) is shown with the condensate fraction,  $\rho_0$  (Eq. 29), as functions of  $\rho$  in Fig. 4. The dashed line is the mean field result for both quantities. At the mean field level,  $\rho_0$  and  $\rho_s$  are identical which is, perhaps, not so surprising. What is surprising is that when we include the spin-waves,  $\rho_0$  is pushed down while  $\rho_s$  is enhanced. As we see from the figure, agreement with numerical results is extremely good.

It is clear from Fig. 4 that for small densities we have  $\rho_s \approx \rho$  and  $\rho_0 \approx \rho$ . This holds well for  $\rho \leq 0.03$  since at this density  $\rho_s$  and  $\rho_0$  are no longer equal.

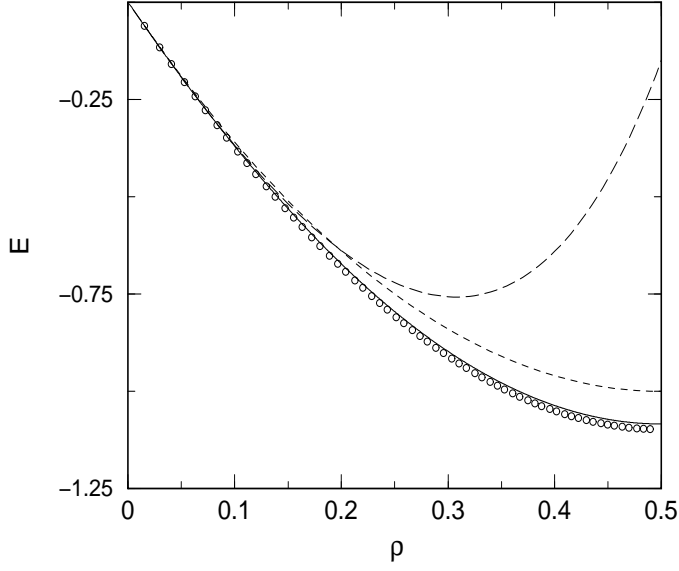


FIG. 1. The boson energy,  $E$ , vs. the density,  $\rho$ . Circles: Simulation results, dashed line: Mean field, solid line: with spin-wave correction, long dashed: Ladder diagram summation of Hines *et. al.*<sup>5</sup>

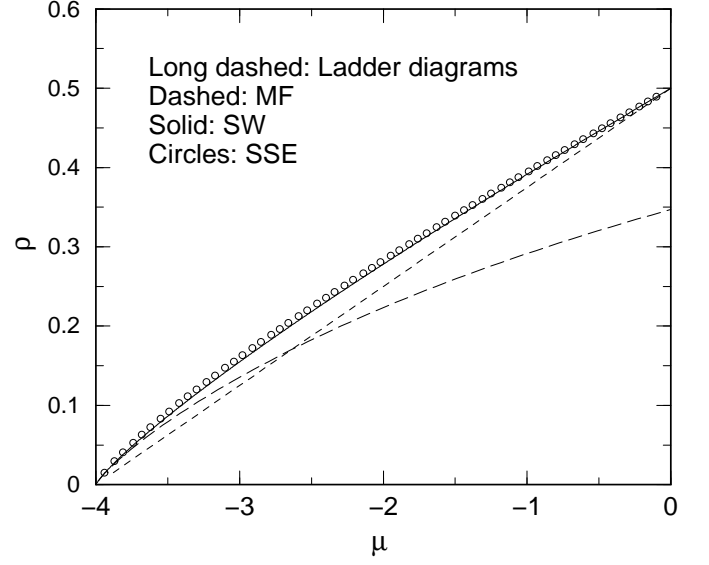


FIG. 3. The particle density,  $\rho$ , vs. the chemical potential,  $\mu$ . Circles: Simulation results, dashed line: Mean field, solid line: with spin-wave correction, long dashed: Ladder diagram summation of Hines *et. al.*<sup>5</sup>

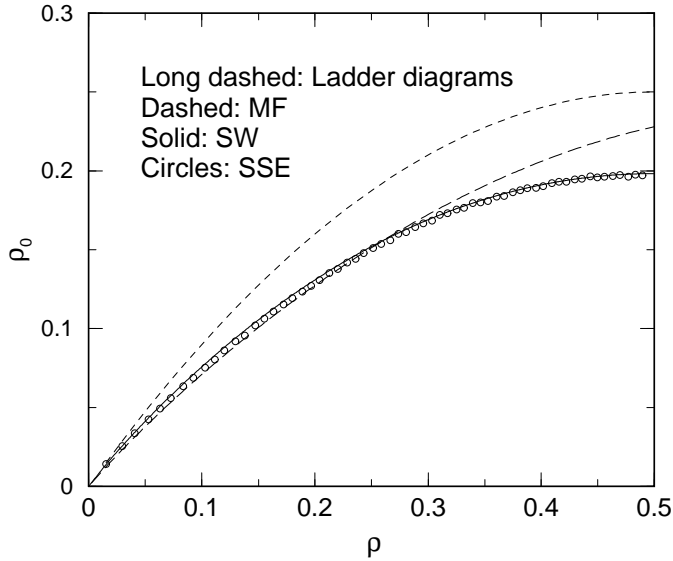


FIG. 2. The condensate fraction,  $\rho_0$ , vs. the density,  $\rho$ . Circles: Simulation results, dashed line: Mean field, solid line: with spin-wave correction, long dashed: Ladder diagram summation of Hines *et. al.*<sup>5</sup>

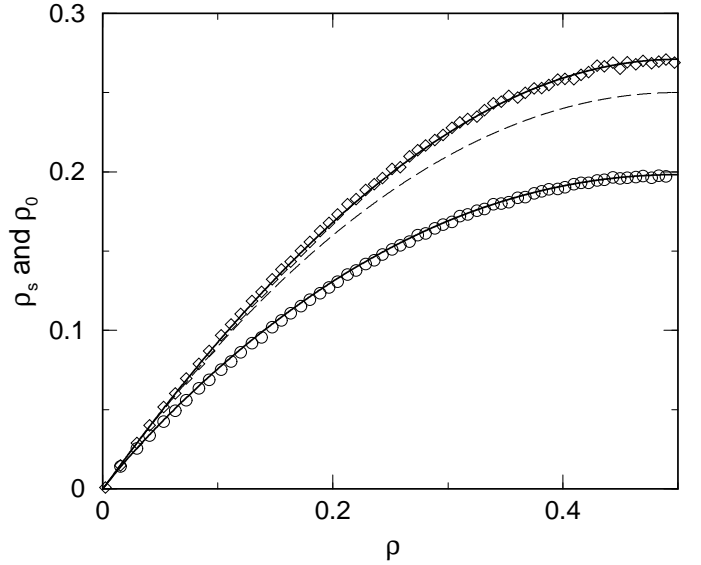


FIG. 4. The dashed line gives both,  $\rho_0$  and  $\rho_s$  vs.  $\rho$ . The numerical results are shown in diamonds,  $\rho_s$ , and circles,  $\rho_0$ . The solid lines are the corresponding spin-wave results.

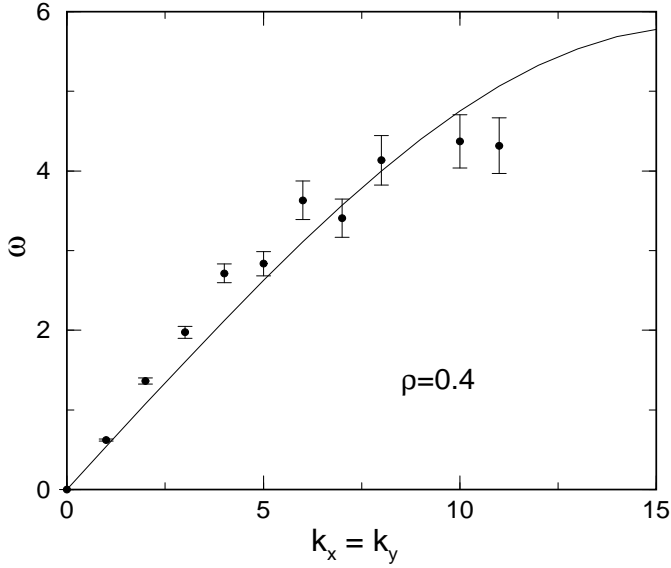


FIG. 5. The excitation spectrum. The solid line is the spin-wave result. It is linear for small  $|\mathbf{k}|$  with a slope (critical velocity)  $c = 2t\sqrt{1 - \left(\frac{\mu}{4t}\right)^2}$ .

As shown in the previous section, the superfluid is stable, the low lying excitations are phononic since the dispersion is linear in  $|\mathbf{k}|$ , Eq. 25. In Fig. 5 we show  $\omega(\mathbf{k})$  for  $\rho = 0.4$ . The solid line is from spin-waves while the circles are the numerical results. Numerically,  $\omega(\mathbf{k})$  was estimated by fitting an exponential to  $\langle a(\mathbf{k}, \tau)a^\dagger(\mathbf{k}, 0) \rangle$  where  $\tau$  is the imaginary time. This quantity is difficult to measure<sup>13</sup>, especially for large momentum vectors, as we see from the noise in the numerical results. It is possible to get better numerical results for this quantity by using more elaborate methods, such as the maximum entropy method.

We see that spin-waves give an excellent description of the system. The agreement between the numerical simulations and the spin-wave calculation is extremely good for all the quantities we considered, except  $\omega(\mathbf{k})$ , where the difficulty is numerical. Furthermore, this agreement extends over the entire density range,  $0 \leq \rho \leq 1$ .

As seen above, the spin-wave results presented here contain momentum sums which we do numerically. We can, however, find simple empirical fits which agree with the simulations at least as well as the spin-wave calculation. The choice of the functional form of the fits was guided by two considerations: (a) Particle hole symmetry which suggests dependence on  $\rho(1 - \rho)$ , and (b) the low density diagrammatic results in the continuum (see next section). So, we found the following fits for the boson energy per site:

$$E_{fit} = \rho(1 - \rho) \left( \frac{4\pi\rho(1 - \rho)}{|\ln(A\rho(1 - \rho))|} \left( 1 - B \frac{\ln|\ln(A\rho(1 - \rho))|}{|\ln(A\rho(1 - \rho))|} \right) - 4 \right), \quad (42)$$

where  $A = 0.537$  and  $B = 3.588$  are the fitting parameters. The condensate density is given by

$$\rho_0^{fit} = \rho(1 - \rho) \left( 1 - \frac{1}{|\ln(0.0335\rho(1 - \rho))|} \right), \quad (43)$$

and superfluid density,

$$\rho_s^{fit} = \rho(1 - \rho) \left( 1 + \frac{0.11245}{|\ln(\rho(1 - \rho))|} \right). \quad (44)$$

We can obtain an equally good fit for the superfluid density using the form

$$\rho_s^{fit} = \rho(1 - \rho) \left( 1 + A\rho(1 - \rho) \right), \quad (45)$$

with  $A = 0.3356$ . To give an idea of the goodness of these fits, we mention that they agree as well with the numerical results as the spin-wave results. It is interesting to note that, although in Fig. 4  $\rho_s$  and  $\rho_0$  appear to have similar functional forms, using Eq. 45 gives very poor results for  $\rho_0$ .

We re-iterate that these fits, Eqs. (42,43,44,45) are purely empirical and are given just as a shortcut to get accurate results.

#### IV. THE CONTINUUM

The excellent agreement we found in the previous section between simulations and spin-waves suggests a comparison with the ladder diagram summation results in the continuum.<sup>4,5</sup> The point is that the continuum results were obtained using approximations that are valid for very low densities, which is where the lattice results should approach the continuum. This should give an idea of the density where the continuum results start to break down. Of course, this breakdown could be due to the breakdown of the validity of the ladder diagram calculation, or to the increasing importance of lattice effects, or both.

Using diagrammatic methods, Schick<sup>4</sup> showed that the condensate density is given by,<sup>20</sup>

$$\frac{1}{2\bar{\rho}_0} = -\text{PP} \int_0^\infty \frac{|f(0, x)|^2 dx}{x^2 - \bar{\mu}}, \quad (46)$$

where PP stands for principal part, and  $\bar{\mu} = 2\mu a^2$ ,  $\bar{\rho}_0 = \rho_0 a^2/\pi$ . The diameter of the hardcore particles is  $a$ . In the lattice simulations this corresponds to the lattice spacing.  $f(\mathbf{q}', \mathbf{q})$  is the scattering amplitude in two dimensions for two particles interacting via the hardcore potential. Schick<sup>4</sup> showed that

$$|f(0, \mathbf{q})|^2 = \frac{16}{[J_0^2(qa) + Y_0^2(qa)]}, \quad (47)$$

where  $J_0^2(qa)$  and  $Y_0^2(qa)$  are Bessel functions of zero order of the first and second kind, respectively. By considering the first few terms in the small argument expansion

of the Bessel functions, Hines *et al* performed the integral Eq. 46 and obtained for the condensate density,<sup>5</sup>

$$\frac{1}{2\bar{\rho}_0} = \frac{-8\pi^2 \ln \bar{\mu}}{\bar{\mu}(\ln^2 \bar{\mu} + \pi^2)} + \frac{16\pi^2(\gamma - \ln 2)(\ln^2 \bar{\mu} - \pi^2)}{\bar{\mu}(\ln^2 \bar{\mu} + \pi^2)^2} + \mathcal{O}\left(\frac{1}{\bar{\mu} \ln^3 \bar{\mu}}\right). \quad (48)$$

Where  $\gamma$  is Euler's constant. Using this equation with the appropriate Green functions<sup>4</sup>, we can obtain the relation between the chemical potential and particle density,

$$\mu = \frac{8\pi\rho}{-\ln\bar{\rho}} \left( 1 - \frac{\ln(-\ln\bar{\rho})}{-\ln\bar{\rho}} + \frac{(2\gamma + \ln 2 + 2\ln\pi - 1)}{-\ln\bar{\rho}} + \frac{\ln^2(-\ln\bar{\rho})}{(-\ln\bar{\rho})^2} - (4\gamma + 2\ln 2 + 4\ln\pi - 1) \frac{\ln(-\ln\bar{\rho})}{(-\ln\bar{\rho})^2} + \mathcal{O}\left(\frac{1}{\ln^2\bar{\rho}}\right) \right). \quad (49)$$

Integrating this equation with respect to the density yields the energy per particle,

$$\epsilon_p = \frac{4\pi\rho}{-\ln\bar{\rho}} \left( 1 - \frac{\ln(-\ln\bar{\rho})}{-\ln\bar{\rho}} + \frac{(2\gamma + \ln 2 + 2\ln\pi - 3/2)}{-\ln\bar{\rho}} + \frac{\ln^2(-\ln\bar{\rho})}{(-\ln\bar{\rho})^2} - (4\gamma + 2\ln 2 + 4\ln\pi - 2) \frac{\ln(-\ln\bar{\rho})}{(-\ln\bar{\rho})^2} + \mathcal{O}\left(\frac{1}{\ln^2\bar{\rho}}\right) \right). \quad (50)$$

Finally, we can also get the condensate density,

$$\rho_0 = \rho \left( 1 - \frac{1}{-\ln(\bar{\rho})} + \mathcal{O}\left(\frac{1}{\ln^2\bar{\rho}}\right) \right). \quad (51)$$

To compare these equations with the spin-wave and simulation results, we should first recall that the kinetic energy term used there is the full Laplacian. On the other hand, for the lattice bosons we did not include the diagonal term of the Laplacian in the kinetic energy. Furthermore, we normalized the energy by the number of sites. So, the simulation and spin-wave energies should be compared with  $\rho(\epsilon_p - 4)$ . With this proviso, Eqs. (49,50,51) are used to calculate the dashed lines in Figs. (1,2,3). We see that in all cases the ladder calculation agrees well with both the lattice simulations and the spin-wave calculations for densities  $0 \leq \rho \leq 0.05$  and sometimes up to  $\rho = 0.1$ . It is interesting to note that these densities are much higher than was thought to be the range of validity of the ladder approximation.<sup>5</sup>

One can also integrate Eq. 46 numerically thus avoiding the asymptotic expansion of the Bessel functions. In figure 6 we show  $\rho_0$  versus  $\mu$  from the numerical integration of Eq. 46 (dashed line) and the spin-wave calculation (solid line). We see that the exact (numerical) calculation of  $\rho_0$  with the ladder approximation does not improve

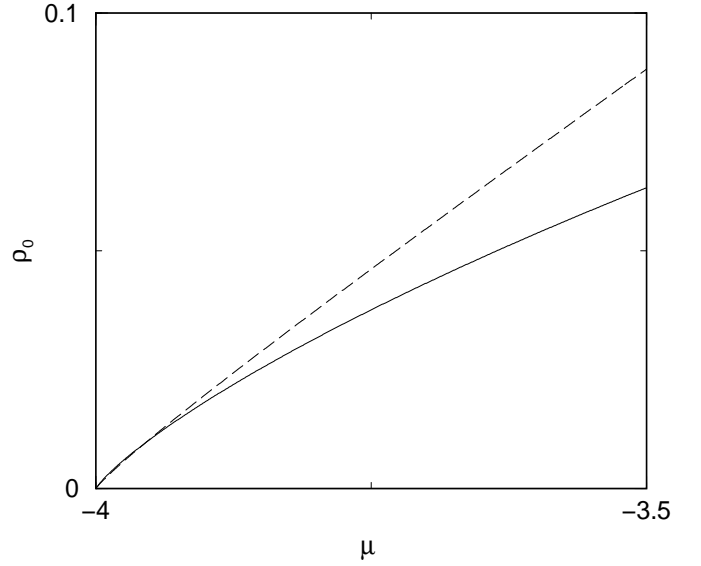


FIG. 6.  $\rho_0$  vs  $\mu$ . The dashed line is the full numerical integration of Eq. 46, the solid line is the spin-wave result for a  $1024 \times 1024$  system.

the comparison with the numerical results. In particular, since this approximation is based on the assumption of very low density, it does not exhibit the particle hole symmetry present in the system.

To demonstrate how agreement between the ladder and spin-wave approximations is approached, we show in Fig. 7 the spin-wave energy, Eq. 30, minus the ladder diagram energy, Eq. 50, versus  $\rho$ . We see that the agreement is indeed excellent and that the difference tends to zero like  $\rho^2$ . To get a clearer idea of the agreement, one should also look at the fractional difference,  $\Delta E/E_{SW} = (E_{SW} - E_{ladder})/E_{SW}$ . For example for  $\rho = 0.022$  we find  $\Delta E/E_{SW} = 1.4 \times 10^{-3}$ , while for  $\rho = 5 \times 10^{-5}$  we find  $\Delta E/E_{SW} = 1.3 \times 10^{-6}$ .

While discussing superfluids in the continuum, we take the opportunity to make some comments regarding the Onsager-Penrose estimate of the condensate density.<sup>21</sup> Often in the literature (see for example reference 22 and references therein) results for the condensate density,  $\rho_0$ , or condensate fraction,  $\rho_0/\rho$ , are compared with the estimate by Penrose and Onsager<sup>21</sup> as the standard calculation. However, the estimate by Penrose and Onsager is incorrect because the trial wavefunction they use is too restrictive: It is unity if the particles do not touch and vanishes if they do touch. In fact, wavefunctions do not vanish so brutally when they approach an infinite wall, they go to zero gradually: They start decreasing *before* the wall is reached. It turns out that this effect, neglected in the calculation of Ref. 21, changes the results a great deal.<sup>23</sup> In three dimensions, according to Ref. 21,  $\rho_0 \approx \rho(1 - (4\pi/3)a^3\rho)$  while using the approach of Bogoliubov<sup>1</sup>, one finds<sup>23</sup>  $\rho_0 \approx \rho(1 - (8/3)\sqrt{(a^3\rho)/\pi})$ , where  $a$  is the diameter of the particles. It so happens that for the physical values present in experiments, both



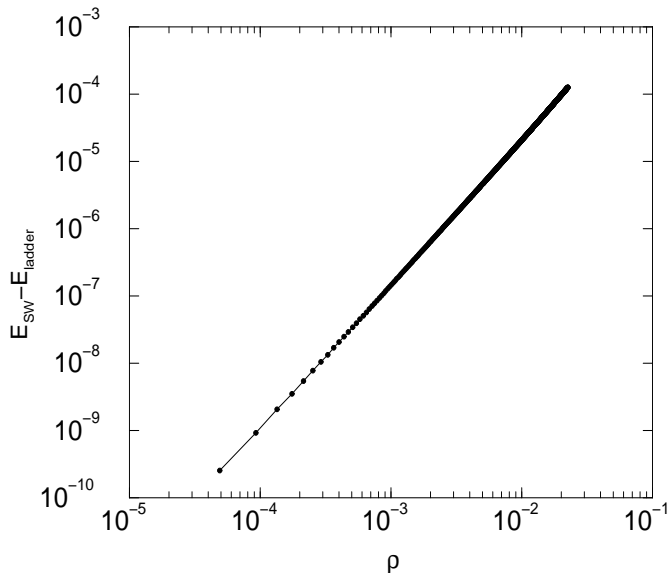


FIG. 7. The difference between the spin-wave and the ladder diagram energies is plotted as a function of  $\rho$ . The difference vanishes like  $\rho^2$ .

estimates give  $\rho_0/\rho$ ) of the order of 10%. However, they give very different functional dependence on the density,  $\rho$ . Similar differences occur in two dimensions, of course.

## V. FINITE TEMPERATURE

In addition to the ground state, we studied the finite temperature Kosterlitz-Thouless transition to superfluidity as a function of the particle density.

To determine the transition temperature,  $T_{KT}$  we exploit the universal jump in the superfluid density shown in Eq. 41. The results are shown in Fig. 8. The simulations were done for  $L \times L$  systems with  $L = 16, 32, 64, 96$  and extrapolated to the thermodynamic limit.

For small, but not too small, particle densities, the bosons behave approximately like free particles which should give  $\rho_s \propto \rho$ . The simulations, Fig. 8, confirm this. We get,

$$\rho_s \frac{\pi \hbar^2}{2m} = k_B T_{KT} \simeq 0.740(2) \frac{\pi \hbar^2}{2m} \rho. \quad (52)$$

On the other hand, for very low densities, and consequently very low  $T_{KT}$ , we should see a crossover to a nonlinear regime when the correlation length,  $\xi$ , exceeds the mean interparticle distance,  $\rho^{1/d}$ . Using the results of Fisher and Hohenberg<sup>24</sup>, the  $\rho$  dependence of  $T_{KT}$  in this limit is given by

$$k_B T_{KT} \simeq \frac{4\pi \hbar^2 \rho}{2m \ln(1/(\rho a^2))} \quad (53)$$

where  $a$  is the scattering length, equal to one lattice spacing in the case of hardcore bosons. Using equations 52

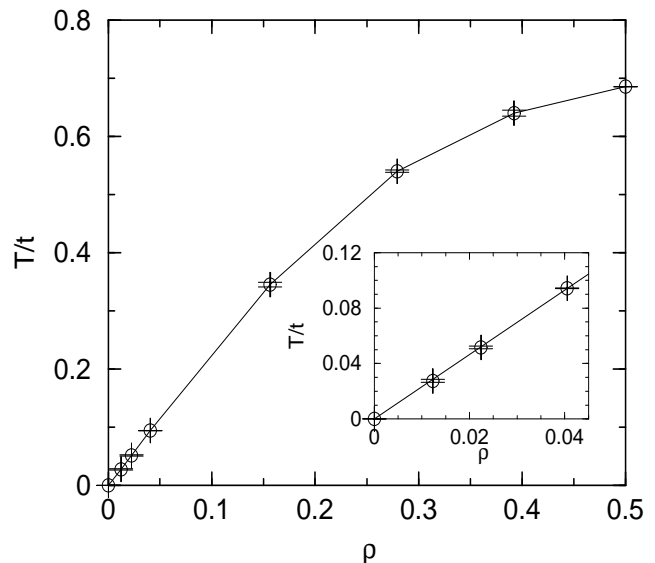


FIG. 8. The critical temperature,  $T_{KT}$ , as a function of the particle density. The inset shows  $T_{KT}$  for a small density range  $0 \leq \rho \leq 0.045$ .

and 53, we get an estimate for the upper bound of the density at which the crossover occurs,

$$\rho a^2 < e^{-e^{4/0.740(2)}} < 10^{-90}. \quad (54)$$

A value which is far too small to be tested numerically. This gives some limit on the usefulness of the result of Fisher and Hohenberg.

## VI. CONCLUSIONS

By direct comparison with numerical simulations, we have shown that spin-waves describe extremely well the properties of hardcore bosons, or equivalently spin-1/2 Heisenberg antiferromagnet in a magnetic field. This remarkable agreement extends over the entire density range,  $0 \leq \rho \leq 1$ .

This verification of the accuracy of the spin-wave approach in the absence of interactions other than hardcore contact, offers a measure of confidence in the accuracy of such an analysis even in the presence of near and next near interactions.<sup>8</sup> We believe a mean field plus spin-wave approach should still work well in this case. A direct comparison with numerical simulations would, however, offer more conclusive assurance. Of course, the quality and reliability of the spin-wave calculation depends strongly on the mean field states that are assumed therein lies the challenge. In the case of pure hardcore repulsion, the mean field state was easy to guess: Uniform particle density. However, the presence of competing interactions, such as near (nn) and next near (nnn) neighbors, can complicate things. For example, if the nn interaction dominates, it seems reasonable to use a

checkerboard density wave as the mean field state. However, there are some other exotic states that might lower the energy and need to be examined. One such candidate is the bond-ordered state.<sup>25</sup>

The agreement between the spin-waves and the ladder diagram approximation for small densities, not only bears out the exact leading term of the energy,  $\epsilon(\rho) = 4\pi\rho(\hbar^2/2m)|\ln(\rho a^2)|^{-1}$ , but also agrees very well with the logarithmic corrections. For example, Eq. 50 agrees very well with the numerical results, Fig. 1, up to  $\rho \approx 0.12$ , whereas, keeping only the leading contribution, deviations are observed at  $\rho \approx 0.07$ . In other words, the numerical results are accurate enough to probe the logarithmic corrections. It would therefore be interesting to compare numerical simulations of hard-core bosons in the continuum with our spin-wave calculation for large densities. We could not find such simulations in the literature. One interesting question in that regard is whether the continuum limit of the spin-wave equations accurately describes bosons in the continuum. In that case, the spin-wave approach would offer an alternate simpler way to calculate the continuum case.

Finally, we also determined the KT transition temperature,  $T_{KT}$ , as a function of particle density. We found that the theoretically predicted behavior<sup>24</sup> appears to be valid at such exceedingly small values as to preclude numerical and experimental verification.

#### Acknowledgments

We acknowledge very useful conversations with F. Hébert, M. Le Bellac and R. T. Scalettar. We also thank ETH-Zurich and HLRS (Stuttgart) for very generous grants of computer time.

- <sup>6</sup> E.H. Lieb and J. Yngvason, math-ph/0002014.
- <sup>7</sup> K.-S. Liu and M. E. Fisher, J. Low Temp. Phys. **10**, 655 (1973)
- <sup>8</sup> R. T. Scalettar, G. G. Batrouni, A. P. Kampf and G. T. Zimanyi, Phys. Rev. **B51**, 8476 (1995).
- <sup>9</sup> G. Murthy, D. Arovas and A. Auerbach, Phys. Rev. **B55**, 3104 (1997).
- <sup>10</sup> G. G. Batrouni and R. T. Scalettar, Phys. Rev. Lett. **84**, 1599 (2000).
- <sup>11</sup> F. Hebert, G. G. Batrouni, R. T. Scalettar, G. Schmid, M. Troyer and A. Dorneich, cond-mat/010545.
- <sup>12</sup> A. Sandvik, Phys. Rev. **B59**, R14157 (1999).
- <sup>13</sup> A. Dorneich and M. Troyer, cond-mat/0106471.
- <sup>14</sup> See for example S.-K. Ma, *Statistical Mechanics*, World Scientific, Singapore.
- <sup>15</sup> Y.-C. Cheng, Phys.Rev. **B23**, 157 (1981).
- <sup>16</sup> M. E. Fisher, M. N. Barber, and D. Jasnow, Phys. Rev. **A8**, 1111 (1973).
- <sup>17</sup> D. M. Ceperley and E. L. Pollock, Phys. Rev. **B39**, 2084 (1984).
- <sup>18</sup> J. M. Kosterlitz and D. J. Thouless, Prog. Low Temp. Phys. **VIIB** (1978).
- <sup>19</sup> We thank R. Kaiser for drawing our attention to this.
- <sup>20</sup> To compare this equation with those of references 4 and 5, one should keep in mind that in our case,  $t = \hbar^2/(2m) = 1$ . Schick takes  $\hbar = 1$  and displays  $m$  explicitly, while Hines *et al* take  $\hbar = m = 1$ .
- <sup>21</sup> O. Penrose and L. Onsager, Phys. Rev. **104**, 576 (1956).
- <sup>22</sup> D. M. Ceperley, Rev. Mod. Phys. **67**, 279 (1995); P. A. Whitlock, D. M. Ceperley, G. V. Chester and M. H. Kalos, Phys. Rev. **B19**, 5598 (1979).
- <sup>23</sup> M. Le Bellac and Ph. Nozières, unpublished (private communication).
- <sup>24</sup> D. Fisher and P. C. Hohenberg, Phys. Rev. **B37**, 4936 (1988).
- <sup>25</sup> N. Read and Subir Sachdev, Phys. Rev. Lett. **62**, 1694 (1989); Kwon Park and Subir Sachdev, cond-mat/0104519; Subir Sachdev, cond-mat/0108238.

---

<sup>1</sup> N.N. Bogoliubov, J. Phys. (U.S.S.R.) **11**, 23 (1947); N.N. Bogoliubov and D.N. Zubarev, Sov. Phys.-JETP **1**, 83 (1955).

<sup>2</sup> K. Huang and C.N. Yang, Phys. Rev. **105**, 767 (1957); T.D. Lee, K. Huang, and C.N. Yang, Phys. Rev. **106**, 1135 (1957); K.A. Brueckner and K. Sawada, Phys. Rev. **106**, 1117 and 1128 (1957); S.T. Beliaev, Sov. Phys.-JETP **7**, 299 (1958); T.T. Wu, Phys. Rev. **115**, 1390 (1959); N. Hugenholtz and D. Pines, Phys. Rev. **116**, 489 (1959); M. Girardeau and R. Arnowitt, Phys. Rev. **113**, 755 (1959); T.D. Lee and C.N. Yang, Phys. Rev. **117**, 12 (1960); E.H. Lieb, Phys. Rev. **130**, 2518 (1963).

<sup>3</sup> E.H. Lieb and J. Yngvason, Phys. Rev. Lett. **80**, 2504 (1998).

<sup>4</sup> M. Schick, Phys. Rev. A **3**, 1067 (1971).

<sup>5</sup> D.F. Hines, N.E. Frankel and D.J. Mitchell, Phys. Lett. **68A**, 12 (1978).